ELSEVIER

Nuclear Instruments and Methods in Physics Research A 463 (2001) 250–267

NUCLEAR INSTRUMENTS & METHODS IN PHYSICS RESEARCH Section A

www.elsevier.nl/locate/nima

Review of the Shockley–Ramo theorem and its application in semiconductor gamma-ray detectors

Zhong He*

Department of Nuclear Engineering and Radiological Sciences, University of Michigan, Ann Arbor, MI 48109, USA

Received 10 July 2000; received in revised form 7 November 2000; accepted 14 November 2000

Abstract

The Shockley–Ramo theorem is reviewed based on the conservation of energy. This review shows how the energy is transferred from the bias supplies to the moving charge within a device. In addition, the discussion extends the original theorem to include cases in which a constant magnetic field is present, as well as when the device medium is heterogeneous. The rapid development of single polarity charge sensing techniques implemented in recent years on semiconductor γ-ray detectors are summarized, and a fundamental interpretation of these techniques based on the Shockley–Ramo theorem is presented.

PACS: 07.85.Nc; 07.85.−m

Keywords: Shockley–Ramo theorem; Radiation detectors; Single polarity charge sensing; X- and γ-ray spectrometers; Wide band-gap semiconductors; Position sensitive detectors

1. Review of the Shockley–Ramo theorem

1.1. Introduction

The common principle of a wide range of radiation detection techniques can be described as follows: the incoming radiation generates free-moving charge q within the detection apparatus, and then the charge Q induced on an electrode by the movement of q is amplified and converted to the output signal. Because of the unique relationship between the energy deposited by the radiation to the moving charge q generated in the device, and between the induced charge Q on the electrode and the output signal, the deposited energy can be obtained from the output pulse amplitude. The general relationship between these quantities is illustrated below:

Deposited energy → Moving charge q → Induced charge Q → Output signal.

We can understand this process by considering an example of a γ-ray spectrometer using semiconductors. The incident γ-ray interacts with the semiconductor and generates a large number of electron–hole pairs proportional to the deposited energy. The movement of these electrons and holes due to the electric field within the device, which

*Tel.: +1-734-763-7130; fax: +1-734-763-4540.
E-mail address: hezhong@umich.edu (Z. He).

0168-9002/01/$ - see front matter
PII: S0168-9002(01)00223-6

correspond to the q discussed above, cause variation of induced charge Q on an electrode. The change of Q is converted to a voltage pulse using a charge sensing amplifier and the amplitude of the output voltage signal ideally is proportional to the deposited energy.

The time dependent output signal of a charge sensing device can be predicted if the induced charge Q on the readout electrode can be calculated as a function of instantaneous position of the moving charge q within the device. Prior to the Shockley–Ramo Theorem, one had to calculate the instantaneous electric field $\boldsymbol{E}$ when the moving charge q is at each point of its trajectory, and then calculate the induced charge Q by integrating the normal component of $\boldsymbol{E}$ over the surface S surrounding the electrode:

$$Q = \oint_S \varepsilon \boldsymbol{E} \cdot \mathrm{d}\boldsymbol{S}$$

where ε is the dielectric constant of the medium. This calculation process is very tedious since large numbers of $\boldsymbol{E}$, which correspond to different locations of q along its trajectory, needed to be calculated to obtain good precision. Shockley [1] and Ramo [2] independently found a simpler method of calculating the induced charge on any electrode of a vacuum tube. Later, it was proven [3,4] that the Shockley–Ramo theorem can be applied not only to vacuum tubes, which can be considered as having no space charge within the apparatus, but is also valid in the presence of stationary space charge. This generalization leads to wider application of the theorem in predicting output signals from many types of charge sensing devices.

1.2. The Shockley–Ramo theorem

The Shockley–Ramo theorem states: The charge Q and current i on an electrode induced by a moving point charge q are given by:

$$Q = -q\varphi_0(\boldsymbol{x})$$

$$i = q\boldsymbol{v} \cdot \boldsymbol{E}_0(\boldsymbol{x})$$

where $\boldsymbol{v}$ is the instantaneous velocity of charge q. $\varphi_0(\boldsymbol{x})$ and $\boldsymbol{E}_0(\boldsymbol{x})$ are the electric potential and field that would exist at q's instantaneous position $\boldsymbol{x}$ under the following circumstances: the selected electrode at unit potential, all other electrodes at zero potential and all charges removed.

φ_0 and $\boldsymbol{E}_0$ are called the weighting potential and the weighting field, respectively. While the trajectory of the charge q is determined by the actual operating electric field, the induced charge Q can be calculated much easier with the help of the weighting field. Because there is only one field that must be calculated, which is independent of the moving charge q, and the space charge is not involved. The original Shockley–Ramo theorem makes the usual assumptions that the magnetic effects are negligible and the electric field propagates instantaneously. Under these assumptions, the problem can be treated as electrostatics at each moment of charge movement.

1.3. An important corollary: the charge induced by q is independent of applied potentials on electrodes and the space charge

An actual device is illustrated in Fig. 1(a). It has a number of electrodes kept at constant voltages V_i $(i = 1, 2, \ldots, K)$, a moving charge q and stationary space charge $\rho(\boldsymbol{x})$ which is represented by the darker background within the device. The surface S of the volume τ is surrounded completely by surfaces S_i $(i = 1, 2, \ldots, K)$ of electrodes. The most outside boundary can be either the surface of a conductor at potential V_K or at infinity with zero potential ($V_K = 0$ V) corresponding to an open apparatus. The electric potential $\varphi(\boldsymbol{x})$ within the device satisfies Poisson's equation with Dirichlet boundary conditions, and the electric field $\boldsymbol{E}(\boldsymbol{x}) = -\nabla\varphi(\boldsymbol{x})$ is uniquely determined:

$$\begin{aligned} &\nabla^2\varphi(\boldsymbol{x}) = -[\rho(\boldsymbol{x}) + q\delta(\boldsymbol{x} - \boldsymbol{x}_q)]/\varepsilon \\ &\varphi|_{S_i} = V_i, \quad i = 1, 2, \ldots, K \end{aligned} \tag{1}$$

where $\boldsymbol{x}_q$ is the location of the moving charge q and ε is the dielectric constant of the detector medium. From the linear superposition principle,

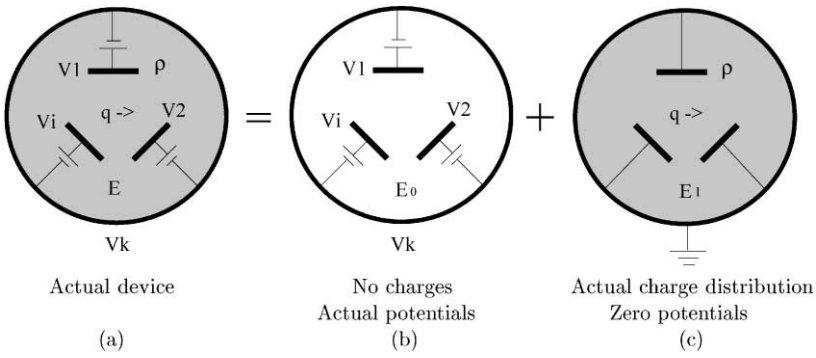

Fig. 1. Application of the linear superposition principle.

let $\varphi = \varphi_0 + \varphi_s + \varphi_q$, where

$$\nabla^2\varphi_0(\boldsymbol{x}) = 0, \quad \varphi_0|_{S_i} = V_i, \quad i = 1, 2, \ldots, K$$

$$\nabla^2\varphi_s(\boldsymbol{x}) = -\rho(\boldsymbol{x})/\varepsilon, \quad \varphi_s|_{S_i} = 0, \quad i = 1, 2, \ldots, K$$

$$\nabla^2\varphi_q(\boldsymbol{x}) = -q \cdot \delta(\boldsymbol{x} - \boldsymbol{x}_q)/\varepsilon, \quad \varphi_q|_{S_i} = 0, \quad i = 1, 2, \ldots, K$$

where φ_0 would be the potential within the device when the electrodes are still kept at the actual voltages but with no charge within the device, φ_s would be the potential generated only by the stationary space charge $\rho(\boldsymbol{x})$ while all electrodes are grounded, and φ_q would be the field only from the presence of the moving charge q while keeping all electrodes at zero voltage. Similarly, the electric field $\boldsymbol{E}$ consists of three components $\boldsymbol{E} = \boldsymbol{E}_0 + \boldsymbol{E}_s + \boldsymbol{E}_q$, where $\boldsymbol{E}_0 = -\nabla\varphi_0(\boldsymbol{x})$, $\boldsymbol{E}_s = -\nabla\varphi_s(\boldsymbol{x})$ and $\boldsymbol{E}_q = -\nabla\varphi_q(\boldsymbol{x})$. The three electric field components correspond to those due to applied voltages, the space charge and the moving charge, respectively.

The induced charge on electrode i can then be written as:

$$Q_i = \oint_{S_i} \varepsilon\boldsymbol{E} \cdot \mathrm{d}\boldsymbol{S}_i = \oint_{S_i} \varepsilon\boldsymbol{E}_0 \cdot \mathrm{d}\boldsymbol{S}_i + \oint_{S_i} \varepsilon\boldsymbol{E}_s \cdot \mathrm{d}\boldsymbol{S}_i + \oint_{S_i} \varepsilon\boldsymbol{E}_q \cdot \mathrm{d}\boldsymbol{S}_i.$$

The first term shows the induced charge due to the coefficients of capacitance between electrodes, which depends on the actual potentials. The second term shows the contribution of space charge. It is evident that only the last term, which corresponds to $\varphi_q(\boldsymbol{x})$, relates to the moving charge q. Therefore, the induced charge produced by q on electrode i, which is $\oint_{S_i} \varepsilon\boldsymbol{E}_q \cdot \mathrm{d}\boldsymbol{S}_i$, cannot depend on the applied potentials V_i on each electrode, nor on the stationary space charge $\rho(\boldsymbol{x})$. In other words, the induced charge on any electrode produced by q depends only on the location of the moving charge and the configuration of the device, and is independent of the actual bias voltages and space charge distribution.

1.4. Proof of the Shockley–Ramo theorem

We now prove the Shockley–Ramo theorem from the conservation of energy. Because of the linear superposition principle, the case in Fig. 1(a) can be divided into two cases shown in Fig. 1(b) and (c). Case (b) keeps the actual potentials, but all charges $(\rho(\boldsymbol{x}) + q)$ are removed. Case (c) keeps the charges, but all electrodes grounded. The electric potential $\varphi_1(\boldsymbol{x})$ of case (c) is equivalent to $\varphi_s(\boldsymbol{x}) + \varphi_q(\boldsymbol{x})$ mentioned in the previous section. In a linear and isotropic medium, the electric displacement is $\boldsymbol{D} = \varepsilon \cdot \boldsymbol{E}$ where the dielectric constant ε is a scalar. The energy density w of the electric field is given by:

$$w = \frac{1}{2}\boldsymbol{E} \cdot \boldsymbol{D} = \frac{1}{2}\varepsilon E^2.$$

The total energy of the electric field is the integral of energy density over the entire volume of τ. From the conservation of energy, this total energy of the field can only be changed by energy

exchanges between the field and the moving charge q (in the form of kinetic energy), and between the field and power supplies.

Imagine a device having the same configuration, space charge distribution and boundary conditions as shown in Fig. 1(c). When the charge q moves from $\boldsymbol{x}_i$ to $\boldsymbol{x}_f$ within such a device, the work done by the electric field is

$$\int_{\boldsymbol{x}_i}^{\boldsymbol{x}_f} q\boldsymbol{E}_1' \cdot \mathrm{d}\boldsymbol{x}$$

where $\boldsymbol{E}_1'$ is $\boldsymbol{E}_1$ excluding q's own field. While the charge q moves from $\boldsymbol{x}_i$ to $\boldsymbol{x}_f$, the induced charges on electrodes redistribute accordingly at the same potential of zero voltage since all conductors are grounded. Therefore, no work is done on the moving induced charges by power supplies (no energy exchange between the detector system and the power supplies). From the conservation of energy, the work done on charge q must come from the energy stored in the field. Therefore:

$$\int_{\boldsymbol{x}_i}^{\boldsymbol{x}_f} q\boldsymbol{E}_1' \cdot \mathrm{d}\boldsymbol{x} = \frac{1}{2}\int_\tau \varepsilon(E_{1i}^2 - E_{1f}^2)\,\mathrm{d}\tau \tag{2}$$

where $\boldsymbol{E}_{1i}$ and $\boldsymbol{E}_{1f}$ are the electric fields in Fig. 1(c) when the point charge q is at its initial ($\boldsymbol{x}_i$) and final ($\boldsymbol{x}_f$) positions, respectively.

In the actual case shown in Fig. 1(a), since $\boldsymbol{E} = \boldsymbol{E}_0 + \boldsymbol{E}_1$, the work done on charge q by the electric field is

$$\int_{\boldsymbol{x}_i}^{\boldsymbol{x}_f} q(\boldsymbol{E}_0 + \boldsymbol{E}_1')\,\mathrm{d}\boldsymbol{x}.$$

In this case, when the induced charge ΔQ_i on each electrode moves between that electrode and the ground due to the movement of q, the total work done on the induced charges by the power supplies is

$$\sum_{i=1}^{K} V_i \Delta Q_i.$$

Applying the conservation of energy in this case, i.e., the work done by the power supplies minus the energy absorbed by the moving charge q should be equal to the increase of energy stored in the field, we have

$$\sum_{i=1}^{K} V_i \Delta Q_i - \int_{\boldsymbol{x}_i}^{\boldsymbol{x}_f} q(\boldsymbol{E}_0 + \boldsymbol{E}_1')\,\mathrm{d}\boldsymbol{x} = \frac{1}{2}\int_\tau \varepsilon[(\boldsymbol{E}_0 + \boldsymbol{E}_{1f})^2 - (\boldsymbol{E}_0 + \boldsymbol{E}_{1i})^2]\,\mathrm{d}\tau. \tag{3}$$

Apply Green's first identity ([5], p. 41)

$$\int_V (\varphi_1 \nabla^2 \varphi_0 + \nabla\varphi_0 \cdot \nabla\varphi_1)\,\mathrm{d}V = \oint_S \varphi_1 \nabla\varphi_0 \cdot \mathrm{d}\boldsymbol{S}$$

where φ_0 and φ_1 can be any arbitrary functions. Notice $\varphi_1|_S = 0$ (all electrodes are grounded in Fig. 1(c)) and $\nabla^2\varphi_0 = 0$ within the device volume τ (there is no space charge in Fig. 1(b)), we have:

$$\int_\tau \boldsymbol{E}_0 \cdot \boldsymbol{E}_1\,\mathrm{d}\tau = \int_\tau \nabla\varphi_0 \cdot \nabla\varphi_1 \cdot \mathrm{d}\tau = \oint_S \varphi_1 \nabla\varphi_0 \cdot \mathrm{d}\boldsymbol{S} - \int_\tau \varphi_1 \cdot \nabla^2\varphi_0 \cdot \mathrm{d}\tau = 0. \tag{4}$$

Therefore

$$\int_\tau \varepsilon[(\boldsymbol{E}_0 + \boldsymbol{E}_{1f})^2 - (\boldsymbol{E}_0 + \boldsymbol{E}_{1i})^2]\,\mathrm{d}\tau = \int_\tau \varepsilon(E_{1f}^2 - E_{1i}^2)\,\mathrm{d}\tau. \tag{5}$$

Eq. (5) means that when charge q moves from $\boldsymbol{x}_i$ to $\boldsymbol{x}_f$, the change of energy of the electric field in Fig. 1(a) is the same as that in Fig. 1(c). This can be interpreted as stating that the energy stored in the actual field $\boldsymbol{E}$ equals the sum of that in $\boldsymbol{E}_0$ and $\boldsymbol{E}_1$, and the energy in $\boldsymbol{E}_0$ is kept constant. Substituting Eqs. (2) and (5) into Eq. (3), we get

$$\sum_{i=1}^{K} V_i \Delta Q_i = \int_{\boldsymbol{x}_i}^{\boldsymbol{x}_f} q\boldsymbol{E}_0 \cdot \mathrm{d}\boldsymbol{x} = -q[\varphi_0(\boldsymbol{x}_f) - \varphi_0(\boldsymbol{x}_i)]. \tag{6}$$

Eq. (6) can be understood as follows: It can be seen from Eq. (3) that the work done on charge q consists of two parts. The first part $\int_{\boldsymbol{x}_i}^{\boldsymbol{x}_f} q\boldsymbol{E}_0 \cdot \mathrm{d}\boldsymbol{x}$ is from the interaction between q and the actual bias potentials. The second part $\int_{\boldsymbol{x}_i}^{\boldsymbol{x}_f} q\boldsymbol{E}_1' \cdot \mathrm{d}\boldsymbol{x}$ is from the interactions between q, the induced charges by q on electrodes and the stationary space charge within the device. This second part comes from the change in energy stored in the field indicated by Eqs. (2) and (5). Therefore, the work done by the power supplies is converted completely to the

kinetic energy of the moving charge q as if q moved from $\boldsymbol{x}_i$ to $\boldsymbol{x}_f$ in the field $\boldsymbol{E}_0$ generated by the actual bias voltages, with all charges removed from the device (in the presence of the same medium). Notice that in a real (non-vacuum) medium, the kinetic energy gained by q from the electric field can be lost in collisions with the medium.

But recalling our earlier result, the induced charge by q is independent of the actual potentials V_i applied on each electrode. Therefore, in order to single out the variation of the induced charge on the electrode of interest while q moves from its initial to final positions, we can choose the potential to be 1 V on this electrode (say electrode L) and zero on all other electrodes. The induced charge by q on electrode L in this simplified setting should be the same as that with actual biases. Considering the dimensions of V_L and φ_0 are canceled, Eq. (6) gives:

$$\Delta Q_L = \int_{\boldsymbol{x}_i}^{\boldsymbol{x}_f} q\boldsymbol{E}_0 \cdot d\boldsymbol{x} = -q[\varphi_0(\boldsymbol{x}_f) - \varphi_0(\boldsymbol{x}_i)]. \quad (7)$$

The $\boldsymbol{E}_0$ and φ_0 in Eq. (7) correspond to the electric field and potential when electrode L is biased at unit potential (dimensionless), all other electrodes grounded and all charges removed. Therefore, $0 \leqslant \varphi_0 \leqslant 1$ and has no dimension. In fact, an arbitrary bias voltage V_L can be assigned to electrode L in computational modeling. The weighting potential is the calculated electric potential divided by V_L. Because φ_0 is proportional to V_L, it is evident from Eq. (6) that the same ΔQ_L will be obtained when charge q moves from $\boldsymbol{x}_i$ to $\boldsymbol{x}_f$. However, letting $V_L = 1$ makes it easier to see how much the induced charge changes as a fraction of the moving charge q. This is the meaning of weighting field.

The induced current on electrode L is then obtained from Eq. (7) as

$$i_L = \frac{dQ_L}{dt} = q\boldsymbol{E}_0 \cdot \frac{d\boldsymbol{x}}{dt} = q\boldsymbol{v} \cdot \boldsymbol{E}_0. \quad (8)$$

We define the space charge free field $\boldsymbol{E}_0$ associated with electrode L at unit potential and all other electrodes at zero potential as the "weighting field", and φ_0 as the "weighting potential". The maximum induced charge on electrode L by q is $-q$ when q is infinitely close to the surface of electrode L where $\varphi_0 = 1$. This result can be understood from the method of images ([5], p. 54) since the mirror-image charge $-q$ is infinitely close to q in this case, and equals the induced charge on electrode L. The minimum induced charge on electrode L by q is 0, when q is infinitely close to the surface of another electrode or at infinity where $\varphi_0 = 0$. The charge q is neutralized by its mirror charge $-q$ when it is near the surface of another conductor. If we set $\varphi_0(\boldsymbol{x}_i) = 0$ in Eq. (7), it is evident that the induced charge on electrode L by $q(\boldsymbol{x})$ is

$$Q_L = -q\varphi_0(\boldsymbol{x}).$$

The Shockley–Ramo theorem is thus proven.

It should be noted that the Shockley–Ramo theorem is just a special case of Eq. (6). For example, if we want to calculate the total induced charge on all electrodes, we can set potentials on all electrodes to be 1. In this case, if the whole volume τ is enclosed by electrodes, $\varphi_0 = 1$ everywhere. The total induced charge on all conductors is $-q$ which is a constant and the individual charges on each electrode are simply redistributed by the motion of q. The total induced current is zero since $\boldsymbol{E}_0 = 0$. This result reflects the continuity equation for current. Finally, note that if the most outside boundary is infinity (an open device), then the potential at infinity is always zero and cannot be set to 1. In this case, the total induced charge on all conductors is less than q ($Q_L = -q\varphi_0(\boldsymbol{x})$ and $\varphi_0(\boldsymbol{x}) < 1$ inside τ.)

1.5. Further discussion

This proof of the Shockley–Ramo theorem allows the presence of a constant magnetic field $\boldsymbol{B}$, such as an external field. There is no energy transfer between the magnetic field and the moving charge q because the force acting on q ($\boldsymbol{f} = q\boldsymbol{v} \times \boldsymbol{B}$) is always perpendicular to the velocity $\boldsymbol{v}$. The work done by the magnetic field $\int_{\boldsymbol{x}_i}^{\boldsymbol{x}_f} \boldsymbol{f} \cdot d\boldsymbol{x} = 0$. The energy component ($w = \frac{1}{2}\boldsymbol{H} \cdot \boldsymbol{B}$) stored in the magnetic field is invariant when $\boldsymbol{B}$ is kept constant. This term is canceled out on the right hand side in Eqs. (2) and (3).

It is implied that the dielectric constant ε may be a function of position. Therefore, the Shockley–Ramo theorem may also be applied to a heterogeneous medium. If the device medium is not isotropic, such as when $\boldsymbol{D} = \varepsilon \cdot \boldsymbol{E}$ and the electric permittivity ε is a tensor, as long as the linear superposition principle still allows the decomposition of the actual case shown in Fig. 1(a) into the two parts in Figs. 1(b) and (c), the Shockley–Ramo theorem should still be valid (since Eq. (4) is always valid). However, the calculation of the weighting potential could be very complex in a non-isotropic medium.

Although this proof assumes that there is only one moving charge q within the device, the result is also valid when multiple moving charges are present. For example, electrons and holes are both generated when a γ-ray deposits its energy in a semiconductor detector. While electrons and holes are moving in opposite directions in the device, the total induced charge on an electrode is simply the sum of induced charges by all moving charges. In these cases, each $\boldsymbol{E}'_{1k}$ on the left of Eq. (2) corresponding to charge q_k includes also the interactions between q_k and all other moving charges.

This proof of the Shockley–Ramo theorem based on the conservation of energy shows how the energy is transferred from external power supplies to the moving charge q in an actual device. It should be kept in mind that the charge induced on an electrode by q is independent of the actual bias voltages on each electrode. For example, some detectors can be operated without external bias [6]. The cathode and the anode can be kept at the same potential (both electrodes can be grounded at zero voltage as illustrated in Fig. 1(c)), the charges generated by radiation can drift in the internal electric field formed by space charge, such as by a p–n junction in a semiconductor device ([7], p. 369–371). The charges induced on each electrode redistribute while the charge q moves, and the change of the induced charge on a specific electrode can be read out using an amplifier for radiation detection. The weighting potential on the electrode of interest is artificially set to 1 (zero potential on all other electrodes) which is different from the actual bias voltage. For example, in a semiconductor device having a p–n junction, electron–hole pairs that are created within the depletion region by the passage of radiation will be swept out of the depletion region by the electric field. The initial energy for sweeping out charges comes from the energy stored in the electric field as shown in Eq. (2), and later, the original electric field (as well as its energy) is restored by the diffusion of electrons and holes.

In order to use the Shockley–Ramo theorem correctly, the implied condition that the field propagates instantaneously during our derivation should be kept in mind. This means that the transit time of the moving charge needs to be much longer than the propagation time of the field across the volume τ. This restriction also requires that the movement of charge q is non-relativistic and the applied bias voltages do not change too fast. This condition is satisfied in almost all practical cases.

The weighting potential $\varphi_0(\boldsymbol{x})$ $(0 \leqslant \varphi_0(\boldsymbol{x}) \leqslant 1)$ provides a convenient way for calculating the induced charge on any electrode of interest. With a given configuration of a device and the specified electrode, only one weighting potential needs to be calculated from the Poisson equation. After the trajectory $\boldsymbol{x}(t)$ of the moving charge q is determined from the actual operating electric field (and magnetic field if there is one), the charge induced on electrode L by q as a function of time can be obtained as $Q_{\mathrm{L}}(t) = -q\varphi_0(\boldsymbol{x}(t))$.

2. Single-polarity charge sensing on wide band-gap semiconductor γ-ray detectors

2.1. Conventional devices using planar electrodes

Semiconductors having high atomic numbers Z and wide band gaps are desired for efficient γ-ray detection operating at room temperatures. HgI_2, CdTe and CdZnTe are materials that have attracted most attention to date. However, due to trapping of charges, the output signal of a conventional detector having planar electrodes depends not only on the deposited energy, but also on the position of that interaction. Therefore, the deposited energy cannot be obtained uniquely from the amplitude of the output signal.

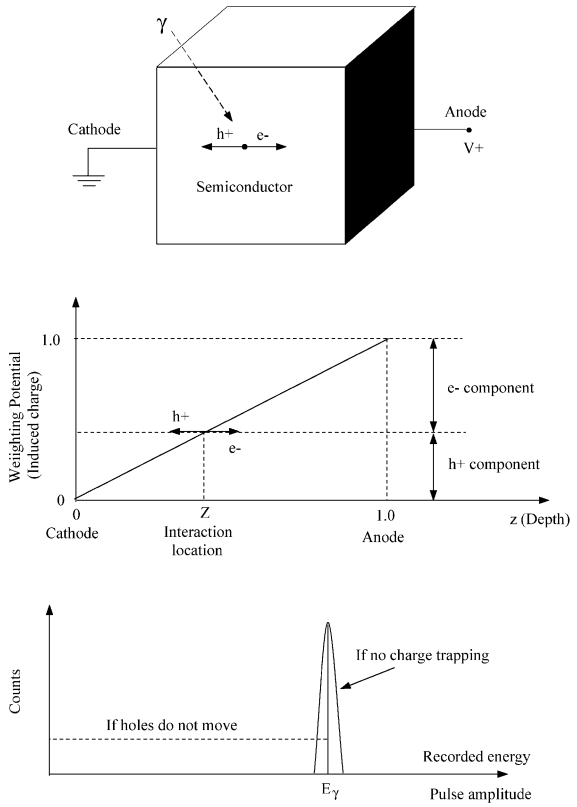

Fig. 2. Illustration of a conventional detector using planar electrodes. Top: The schematic of a semiconductor γ-ray detector using conventional planar electrodes. Middle: The weighting potential of the anode, and signal components from the movements of electrons and holes. Bottom: The expected energy spectra with fixed energy deposition E_γ when the γ-ray interaction depth is distributed uniformly between the cathode and the anode.

The configuration of a conventional detector is illustrated in the top of Fig. 2. When a γ-ray deposits energy within a semiconductor detector, a large number of electron–hole pairs proportional to the energy deposition are generated. Electrons move towards the anode and holes move towards the cathode in the electric field $\boldsymbol{E}$ formed by the bias voltage. The change of induced charge ΔQ on one of the electrodes is converted to a voltage signal by the amplifiers with the pulse amplitude proportional to ΔQ. The weighting potential of the anode (assuming the signal is read out from this electrode) is calculated using the Shockley–Ramo theorem by setting the potential on the anode to 1, and assuming the cathode to be grounded. Recall that the weighting potential is obtained with no space charge. For a slab geometry, the weighting potential is simply a linear function of depth Z from 0 to 1 (assuming the lateral dimension is much larger than the detector thickness) from the surface of the cathode to that of the anode as shown in the middle of Fig. 2

$$\varphi_0(z) = z, \quad 0 \leqslant z \leqslant 1.$$

If the loss of charge carriers during the drift time can be ignored, such as is usually the case in a high purity germanium detector (HPGe), the total change of the induced charge on the anode can be calculated from Eq. (7) while n holes move from $z = Z$ to 0 and n electrons move from $z = Z$ to 1:

$$\Delta Q = -(ne_0)(0 - Z) + (ne_0)(1 - Z) = ne_0$$

where e_0 is the electronic charge and Z is the interaction depth of the γ-ray. The first term is the contribution of holes and the second term is that of electrons. The normalized electron and hole components are shown in the middle of Fig. 2. ΔQ (also the output amplitude) is always proportional to the number of electron–hole pairs generated, which is proportional to the deposited energy, and is independent of the interaction depth. For a constant energy deposition E_γ, the amplitude of the detector output pulse is also constant as shown in the bottom of Fig. 2, and only fluctuates due to the noise of the detector system and the statistical fluctuation in the charge carrier formation. However, when holes can only move very short distance compared to the detector thickness ($\Delta z_h \ll 1$), the induced charge on the anode is

$$\Delta Q_e \approx ne_0(1 - Z) \tag{9}$$

which is depth dependent. If γ-rays interact with detector material at all depths randomly, the induced charge would vary from zero to ne_0 according to Eq. (9). No spectroscopic information can be obtained under these conditions from the pulse amplitude of the detector. The pulse height spectrum corresponding to this case is also shown at the bottom of Fig. 2 for comparison.

Although various pulse processing techniques have been applied to improve the spectroscopic

performance of room temperature semiconductor γ-ray detectors, such as those employed on CdTe devices [8–10], these techniques can lead to significant loss of detection efficiency, especially on thick detectors. This is because none of these signal processing methods can solve the fundamental problem of charge trapping which causes the reduction of signal amplitude that depends on the drift length of charge carriers. With a given noise level of the detector system, the intrinsic signal-to-noise ratio of pulses could approach zero on any detector that has a thickness much larger than the drift length of holes during the charge collection time, when the γ-ray interaction location is close to the anode surface. Therefore, it is impossible to recover the information on γ-ray energy accurately.

In order to overcome the effects of severe trapping of holes in wide band-gap semiconductors, researchers have been investigating techniques in which the pulse amplitude is sensitive only to one type of charge carriers, normally just the electrons (and not the holes). These techniques are called single polarity charge sensing, which can alleviate the charge trapping problem if the drift length of just one type of charge (such as electrons) can be long compared with the detector thickness.

2.2. The Frisch grid technique

The first single polarity charge sensing technique was implemented in gas detectors by Frisch [11] to overcome the problem of slow drift and loss of ions. The Frisch grid is placed very close ($P \ll 1$) to the anode as shown in Fig. 3. Electrons pass through the Frisch grid and are collected by the anode. The weighting potential (φ_0) of the anode is obtained by applying a unit potential on the anode, and zero potential on both the Frisch grid and the cathode. The weighting potential φ_0 is zero between the cathode and the Frisch grid, and rises to 1 linearly from the grid to the anode as shown in the bottom of Fig. 3. This configuration means that the charge moving between the cathode and the grid causes no induced charge on the anode, and only those electrons passed through the grid contribute to the anode signal. Therefore, the output pulse amplitude is proportional to the number of electrons collected, and any induced signal from the movement of charges between the cathode and the Frisch grid, including that from the slow drift of ions, is completely eliminated.

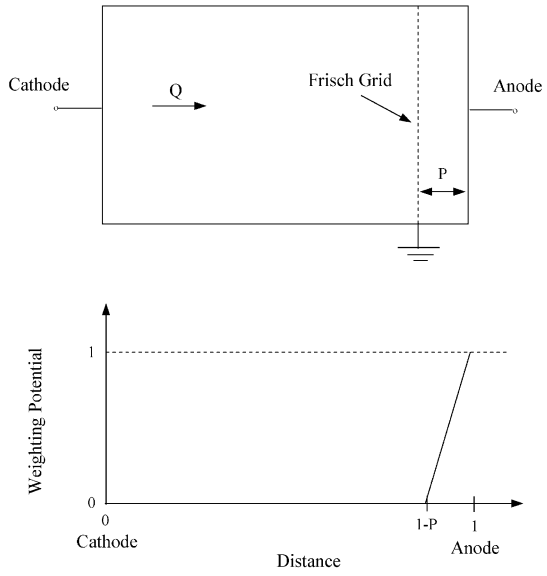

Fig. 3. Side view of a Frisch grid detector and the weighting potential of the anode.

2.3. Coplanar grid electrodes

Single polarity charge sensing was implemented on semiconductor detectors by Luke based on the use of coplanar grid electrodes in 1994 [12,13]. The concept is illustrated in the top of Fig. 4. Instead of a single electrode on the anode, parallel strip electrodes are used and the strips are connected in an alternate manner to give two banks of grid electrodes (electrodes 2 and 3). A voltage difference between these two banks of electrodes is applied so that the selected charge carriers (in this case electrons) are always collected by one electrode, say electrode 2.

The weighting potential φ_2 of electrode 2 within the device is calculated by letting the potential on electrode 2 be 1 and potentials on electrodes 1 and 3 to be zero [14], and solving the Laplace equation (since there is no space charge). Similarly, the weighting potential φ_3 of electrode 3 is calculated

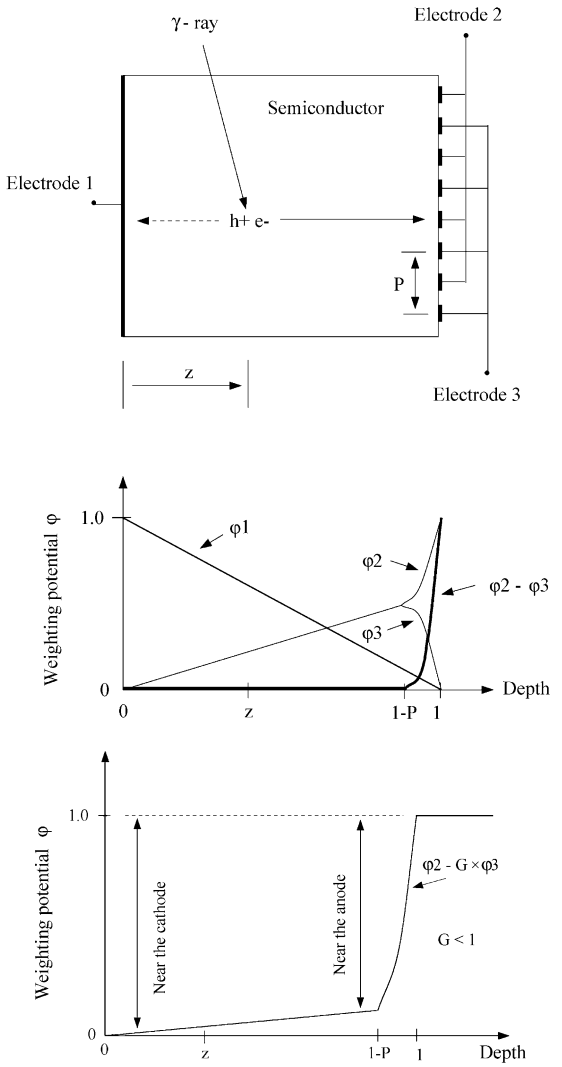

Fig. 4. Illustration of the coplanar grid technique. Top: The side view of a semiconductor γ-ray detector having coplanar grid electrodes. Middle: Illustration of weighting potentials of each electrode. Bottom: The weighting potential of $\varphi_2 - G \times \varphi_3$. The illustration of electron trapping correction using the relative gain compensation technique.

by letting the potential on electrode 3 be 1 and potentials on electrodes 1 and 2 to be zero. The middle of Fig. 4 shows the weighting potentials of each electrode along a line perpendicular to the electrode surfaces and intersecting with one strip of the collecting anode (#2) at its center, such as along the trajectories of electrons and holes shown in the top of Fig. 4. For simplicity, it is assumed that the dimensions of the device parallel to the electrode surfaces are much larger than the detector thickness (normalized to unity). Notice, φ_2 and φ_3 are practically identical for $0<z<1-P$, and then φ_2 approaches 1 and φ_3 drops back to zero rapidly. P is the period of coplanar grid electrodes and is much smaller than the thickness of the device ($P \ll 1$). The characteristic shape of these weighting potentials reflects the fact that the induced charges on electrodes 2 and 3 increase identically due to the symmetry between the two coplanar anodes when electrons move closer (or holes move away) to the anode surface between $0<z<1-P$. This regime is followed by the rapid increase on electrode 2 and drop on electrode 3 back to zero when electrons approach electrode 2 and deviate away from electrode 3 in $z>1-P$ driven by the actual electric field. Single polarity charge sensing is implemented by reading out the difference signal between electrode 2 (collecting anode) and 3 (non-collecting anode). This differential signal corresponds to the weighting potential of $(\varphi_2 - \varphi_3)$. It has zero net value for $0<z<1-P$ and rises from 0 to 1 when a unit charge travels from $z=1-P$ to 1. This $(\varphi_2 - \varphi_3)$ is very similar to the weighting potential of the anode of a gas detector using a Frisch grid shown in the bottom of Fig. 3. If all electrons are collected by the collecting anode and the γ-ray interaction depth is in the region $0 \leqslant Z \leqslant 1-P$, the differential pulse amplitude is proportional to $\Delta Q_2 - \Delta Q_3$ which can be calculated using Eq. (7):

$$\begin{aligned}\Delta Q_{\text{coplanar}} &= \Delta Q_2 - \Delta Q_3 \\ &= n' e_0 \{[\varphi_2(z=1) - \varphi_2(z=Z)] \\ &\quad - [\varphi_3(z=1) - \varphi_3(z=Z)]\}\end{aligned}$$

since $\varphi_2(z=1)=1$, $\varphi_3(z=1)=0$ and $\varphi_2(z=Z)=\varphi_3(z=Z)$, we have

$$\Delta Q_{\text{coplanar}} = n' e_0 \tag{10}$$

where n' is the number of electrons arriving at the surface of coplanar anodes. The induced charge by holes is eliminated since holes move in the linear region of the weighting potentials ($0 \leqslant z \leqslant 1-P$). Since electrons are collected only by the collecting anode (#2) due to the voltage difference between

the coplanar anodes, φ_2 is always equal to 1 and φ_3 equal to zero at $z = 1$ along the actual trajectories of electrons.

If the trapping of electrons is negligible, the amplitude of the differential signal is independent of the depth of the γ-ray interaction and is proportional to the energy deposition of the γ-rays. It should be noted that the differential pulse amplitude has the same pulse height (n_0e_0) as that from a conventional detector using planar electrodes when charge trapping can be neglected. The elimination of the sensitivity of the output pulse to hole motion does not result in any loss of signal amplitude.

In practice, not only holes are severely trapped in wide band-gap semiconductors, but the loss of electrons also cannot be ignored. From our measurements, about 4–10% of electrons can be trapped across 1 cm of currently available CdZnTe at a bias voltage of 1 kV between the cathode and the anode. Therefore, a good γ-ray spectrometer using wide band-gap semiconductors must not only be able to overcome the hole trapping problem, such as by employing a single polarity charge sensing technique, but must also be able to correct for electron trapping. In Luke's differential circuitry, a gain (G) of less than 1 was applied on the non-collecting anode signal before subtraction [12] to compensate for electron trapping. This technique can be understood by observing that the output signal in this case corresponds to the weighting potential of $\varphi_2 - G \times \varphi_3$ which is shown in the bottom of Fig. 4. Applying a gain less than 1 on the non-collecting anode signal effectively reduces the pulse amplitude in a linear relationship as the γ-ray interaction depth becomes closer to the anode surface. Since the loss of electrons is less when the drift length is shorter, this technique compensates the electron trapping if its effects are linear with depth.

It was demonstrated that the coplanar grid technique can significantly improve the energy resolution of a CdZnTe detector [13], with a relatively simple electronic circuitry. Some characteristics of Luke's technique should be noticed: (1) If the number of drift electrons as a function of drift length is an exponential function, the trapping of electrons can be perfectly compensated in most regions of $0 \leqslant z \leqslant 1 - P$, except in the vicinity of the cathode where holes can be collected [15]. This technique works better if the drift length of holes is shorter (more trapping). (2) The weighting potential $\varphi_2 - G \times \varphi_3$ is no longer zero in the region of $0 \leqslant z \leqslant 1 - P$. Therefore, the variation in hole transport can contribute to the fluctuation in the output signal. (3) It can be a challenge to implement coplanar grid electrodes on a large surface. This is rooted from some competing factors. For example, a small pitch of strips is desired to improve the symmetry between coplanar electrodes, to make charge collection more uniform and to reduce the dead region (a layer of thickness P near the coplanar grid surface). However, a small strip pitch increases the capacitance and leakage current between the electrodes, and in turn increases the noise. Smaller gap requires better surface processing to prevent noise breakdown at required bias voltage between coplanar electrodes.

2.4. Other single polarity charge sensing techniques

The earliest single polarity charge sensing technique implemented on semiconductor γ-ray detectors was the development of hemispherical devices [16]. The original strategy was to create a more uniform charge collection by having electrons move in the low field region and holes (having shorter drift length) move in the high field region. On those devices, a small dot anode was placed in the focus of the hemispheric cathode electrode and the signal was read out from the small-area anode. The weighting potential of this small anode can be obtained by applying a unit potential on the anode and grounding the cathode. Because the small scale of the anode relative to the cathode, the weighting potential is very low within most volume of the detector, and rises rapidly to 1 near the anode electrode. Therefore, the induced charge on the anode is dominated by the movement of charge carriers near the anode. For the majority of γ-ray interactions in the device, the pulse amplitude from the small anode is dominated by the number of electrons collected. Although significant improvement in γ-ray energy resolution was demonstrated, the optimum

compensation of the variation of pulse amplitude was not investigated. The most important limiting factor is that the operating electric field is very weak near the cathode where electrons move very slowly. This causes severe charge trapping near the cathode, and limits the effective volume of this type of devices.

A variation of coplanar grid technique was proposed by Amman et al. [17] through which a proper choice of the ratio of strip widths between the collecting and the non-collecting anodes causes the weighting potential of the collecting anode to be the same as that shown at the bottom of Fig. 4. Since the weighting potential corresponding to the sum of induced charges on the collecting and the non-collecting anodes (considering the case of a single anode on a conventional detector) increases linearly from 0 on the cathode surface to 1 on the anode surface, the slow rise from $z = 0$ to $1 - P$ of the weighting potential of the collecting anode indicates that the induced charge on the collecting anode is much smaller than that on the non-collecting anode. This can be implemented if the total area of the collecting anode is much smaller than that of the non-collecting anode. If the trapping of electrons matches the change of the weighting potential in the region of $0 < z < 1 - P$, electron trapping can be compensated. Therefore, signals can be read from just one anode electrode, as simple as a conventional detector, in contrast to reading out two signals and performing subtraction on a coplanar grid configuration. This technique can simplify the readout and reduce electronic noise. However, the electrode configuration, which determines the weighting potential of the collecting electrode, must be designed with given charge trapping properties which are not known accurately on a raw semiconductor material. After the fabrication of the device, the amount of charge trapping can be varied by changing the bias voltage between the cathode and the anode. Therefore, there is only one fixed bias voltage under which the charge trapping is optimally compensated by the weighting potential. The optimum spectroscopic performance of a device is determined not only by the compensation of charge trapping, but also by other factors, such as the leakage current and the amount of charge trapping. Therefore, this technique is not as flexible as a general coplanar device in achieving the best spectroscopic performance. When electron trapping is relatively small, as discussed earlier, the ratio of the areas of the collecting anode to that of the non-collecting anode must also be small. There is a region underneath the non-collecting anode within which the lateral electric field is very weak due to the equipotential on the surface of the non-collecting anode [14]. Electrons in this region tend to be trapped under the non-collecting anode, and they can move out only by thermal diffusion. This effect causes more electron trapping if the energy is deposited underneath the non-collecting anode [17]. Efforts must be paid to minimize the width of the non-collecting anode of these devices.

Patt et al. [18] suggested the use of the electrode structure of a silicon drift detector on HgI_2 detectors. The electric field formed by a set of focusing electrodes drives the electrons to a small anode where they are collected. The principle of this technique can also be understood easily with the help of the weighting potential. The weighting potential of the small anode is calculated by applying a unit potential on the anode and zero on all other electrodes. It is evident that this weighting potential is similar to that shown at the bottom of Fig. 4, with very low values in most of the volume of the detector, and sharply rising to 1 in the immediate vicinity of the small anode. This shape results from the small dimension of the collecting anode and the closeness of the nearest focusing electrode to the collecting anode. Because the nearest focusing electrode forces the weighting potential of the collecting anode to be zero very close to the collecting anode, the induced charge on the small anode is dominated by the number of electrons collected. This technique was demonstrated on a HgI_2 detector having a thickness of 2 mm and an area of 2.5 cm^2. An energy resolution of 0.9% FWHM at 662 keV γ-ray energy was obtained, which is a significant improvement over a conventional planar detector [18]. However, more investigation is needed to understand the reported results. For example, the effective volume of the device which contributed to the photopeak events was not measured. The high continuum in the ^{137}Cs γ-ray energy spectrum between the

photopeak and the Compton edge and at lower energies indicated significant electron trapping within the detector.

Butler [19] proposed the use of a small-area anode surrounded by a 'control electrode' on the same surface of the anode. The principle of this device is very similar to that of Patt et al. applied on HgI_2 detectors. The bias voltages on the anode, the control electrode and the cathode form the operating electric field which drives the electrons towards the small anode. In terms of the weighting potentials, the function of the control electrode is to set the boundary condition to be zero potential on the surface covered by this control electrode. This effectively reduces the weighting potential of the small anode in the detector volume away from the anode and causes the induced charge to be dominated by the movement of electrons near the small anode. Similarly, the shape of the weighting potential of the collecting anode is close to that shown at the bottom of Fig. 4. However, in contrast to the weighting potential of the coplanar grids, this weighting potential in the region from $z = 0$ to $1 - P$ (where P is roughly the relative dimension of the anode electrode to the thickness of the detector) is not linear and in general varies as a function of lateral position even at the same depth. Therefore, an accurate compensation of charge trapping using the weighting potential is more difficult, especially on a detector having large detection volume in which the charge trapping is significant. Furthermore, this technique has the same disadvantage of the single electrode readout technique proposed by Amman et al. [17] that the optimum operating voltage is determined by the configuration of the electrodes. There is no flexibility in varying the optimum operating voltage after the fabrication of the device.

The direct application of the Frisch grid technique to room temperature semiconductor devices was demonstrated on CdZnTe detectors by McGregor et al. [20] and Lee et al. [21]. A pair of Frisch grids were fabricated in parallel on opposite surfaces of thin CdZnTe detectors near the anode. The cathode is biased negative and the anode is biased positive relative to the Frisch grids. The signal is read out from the anode and its amplitude is proportional to the number of electrons collected. The weighting potential of the anode is calculated by applying a potential of 1 on the anode and zero on both the Frisch grid and the cathode. The weighting potential is similar to that shown in Fig. 3. An energy resolution of about 2.7% FWHM at 662 keV γ-ray energy was obtained on a 1 cm^3 CdZnTe detector having a trapezoid prism shape which enhances the spectroscopic performance from the geometric effect [22]. The advantage of this technique is simple readout. Since there is no compensation for charge trapping using the weighting potential, the trapping of electrons will degrade energy resolution on these devices unless a position sensing technique is employed. Another limitation of this method is that the separation distance between the pair of Frisch grids must be kept small to maintain the good shielding of induced signal on the anode while charge carriers move between the cathode and the Frisch grids. This limits the detector volume of a single device.

2.5. A depth sensing technique using the effect of charge trapping

It is sometime desired to know the depth of γ-ray interaction, such as for γ-ray imaging applications, background rejection, and correction for charge trapping. He et al. [23,24] proposed to read out signals simultaneously from both the cathode and the coplanar grid anodes for each γ-ray event. The position of γ-ray interaction between the cathode and the anode then can be obtained from the ratio between these two signals. This is because the weighting potentials are different. For example, the hole mobility is usually much smaller than that of electrons in CdZnTe. A shaping time, which is long compared to the electron drift time and short relative to the hole drift time, can be applied on the cathode signal to obtain the electron component of the induced charge shown in the middle of Fig. 2. As discussed before, the cathode signal is described by Eq. (9). The deposited energy can be obtained from the coplanar anode signal which is described by Eq. (10). The depth of γ-ray interaction is obtained from the ratio of the cathode and the coplanar

anode signals:

$$\frac{\Delta Q_e}{\Delta Q_{\text{coplanar}}} = \frac{n}{n'}(1 - Z) \approx 1 - Z, \quad \text{when } n \approx n'.$$

This technique offers some advantages: (1) It provides the depth of γ-ray interaction as an independent parameter, therefore, it can correct for electron trapping as an arbitrary function of electron drift length. (2) It enables the use of equal gain between the collecting and the non-collecting anodes. This makes the differential weighting potential (see $\varphi_2 - \varphi_3$ in Fig. 4) exactly zero within most detector volume ($0 \leqslant z \leqslant 1 - P$). Therefore, the induced charge of holes can be completely eliminated. In contrast, if a relative gain between coplanar anodes is used, the variation of hole transport properties and weighting potentials at different lateral positions of the same depth will contribute to the fluctuation of pulse amplitude. (3) Since this technique allows the use of equal gain between the two coplanar anodes, the amplitude of the coplanar anode signal is only proportional to the number of electrons collected, and is independent of the shape of the anode weighting potentials (as long as they are identical in $0 \leqslant z \leqslant 1 - P$). This allows the employment of a third anode (boundary electrode) which can help to minimize the difference between weighting potentials of the first two coplanar anodes in the region $0 \leqslant z \leqslant 1 - P$ [25,26]. The introduction of the third anode also allows radial sensing in the region close to the anode surface. An application of this technique is to measure the difference of weighting potentials between the central two coplanar grid anodes which causes poor energy resolution [25]. Since such a detector is both a conventional (the cathode signal) and a single polarity charge sensing detector, it should work better than either type (conventional or single polarity charge sensing) alone simply because it provides more information.

2.6. Strip electrodes

Semiconductor detectors using strip electrodes were first motivated for two-dimensional position sensing [27,28], and it was later realized that single polarity charge sensing can also be achieved by reading out signals from individual strip electrodes [14,27,28]. The induced charge on any particular strip is very low when charge carriers move far away (when the distance to the strip is much larger than the pitch of strip electrodes) from the electrode. This can be understood by noting that the weighting potential of the specific strip electrode is determined by applying a unit potential on the strip electrode and zero potential on all other electrodes. The weighting potential is very low in most of the detector volume except very close to the strip electrode. Therefore, the weighting potential of a strip electrode is very similar to that shown at the bottom of Fig. 4 [14]. If the linear increase of the weighting potential in the region $0 \leqslant z \leqslant 1 - P$ matches the loss of electrons, the expected pulse amplitude remains approximately constant, independent of the drift distance of electrons. Therefore, the spectroscopic performance can be significantly improved. Although the implementations of individual strip readout and the relative gain compensation technique on coplanar grid electrodes look very different, their principles of single polarity charge sensing can be unified by the similarity of their weighting potentials. However, a fundamental difference between the two techniques is that the gain G of the relative gain compensation method can be easily adjusted according to the actual loss of electrons at any given bias voltage between the cathode and the anode, to achieve the optimum compensation. In contrast, the change of the weighting potential in the region $0 \leqslant z \leqslant 1 - P$ is fixed by the configuration of strip electrodes. The optimum electron trapping compensation can only be realized at a particular bias voltage. This is a severe limitation because strip detectors are usually designed not for optimum performance in spectroscopy, but more for imaging applications. Therefore, the pre-determined bias voltage, which can best compensate for charge trapping, is not usually employed due to other constraints.

The application of strip detectors has been mainly for two-dimensional position sensing with fewer readout channels (2N) compared to that of pixellated anode array (N^2) [29]. Orthogonal strips can be used on the anode and the cathode surfaces, respectively [27,28], where one group of strip

electrodes provides the coordinate in x direction and the other provides the y coordinate. Because the weighting potential of one strip electrode increases rapidly to 1 only in the immediate vicinity of the strip, the arriving of electrons on one (or a few) anode strip provides the position in one direction, and the arriving of holes on one (or a few) cathode strip gives the position in another direction. As a consequence, the good position sensitivity depends on the good collection of electrons on the anode surface and also on the efficient collection of holes on the cathode surface. Because the drift length of holes is very short (in the order of $\sim$ 1 mm) in commercially available CdZnTe crystals, the strip readout technique has only been employed on thin ($\sim$ 2 mm) CdZnTe detectors. The employment of this method is more advantageous if both electron and hole drift lengths are long compared to the detector thickness, such as in a high purity Ge detector or if the drift length of holes in CdZnTe could be improved.

2.7. Pixellated anode array

Detectors using pixellated anode arrays were also motivated for two-dimensional position sensitive imaging applications [30,31]. It was found that γ-ray energy resolution obtained from individual anode pixels on a CdZnTe detector was significantly improved compared to that from a conventional detector using planar electrodes. It was soon realized that reading out signals from individual small anode pixels of an anode array is another form of single polarity charge sensing [32]. The principle is very similar to that of using strip electrodes. The induced charge on a particular anode pixel from the moving charge q is very small when q is far away (the distance to the pixel is much greater than the pixel dimension) due to charge sharing among many anode pixels, and increases rapidly when q is in the vicinity of this pixel. The weighting potential of an anode pixel along a line passing through the center of the pixel is similar to the one shown at the bottom of Fig. 4. It increases slowly in the region $0 \leqslant z \leqslant (1 - P)$ and rapidly rises to 1 from $z = 1 - P$ to 1, where P is the relative dimension (to the detector thickness) of one anode pixel. Because the smaller area of an anode pixel compared to that of an anode strip (assuming the same width), the increase of the weighting potential from $z = 0$ to $(1 - P)$ is much lower. The smaller the ratio between the dimension of each anode pixel to the thickness of the detector, the lower the increase of the weighting potential from $z = 0$ to $(1 - P)$. The induced charge on each anode pixel is then contributed mostly from the drift of charges in the immediate vicinity near the pixel. This is called the small pixel effect.

For the same reasons as the strip detectors, most room temperature semiconductor γ-ray detectors using pixellated anode arrays have been designed for imaging applications, not for optimum γ-ray spectroscopy. The pixel dimensions and detector thickness are usually determined based on the requirements on position resolution and energy range of the incoming γ-rays, respectively. Therefore, the weighting potentials of pixel electrodes are fixed by considerations not for spectroscopy. As discussed previously, there is only one bias voltage under which the trapping of charges can be optimally compensated by the slow increase of the weighting potential in the region from $z = 0$ to $(1 - P)$. This is usually not the operating bias voltage used. However, if the optimum bias voltage can be carefully selected, the variation of pulse amplitude due to charge trapping can be significantly reduced from the compensation effect of the weighting potential, and the spectroscopic performance can be improved [33]. The best spectroscopic performance to date obtained at room temperature on a detector using pixellated anode array has been reported by Cook et al. [34].

2.8. Three-dimensional position sensitive detectors

The first fully functional three-dimensional position sensitive semiconductor γ-ray spectrometers were demonstrated on two 1 cm^3 cube CdZnTe detectors by He et al. [35]. The configuration of the pixellated anode array is illustrated in Fig. 5(a). By combining two-dimensional position sensing using a pixellated anode array yielding good energy resolution from the small pixel effect, and the depth sensing technique discussed in

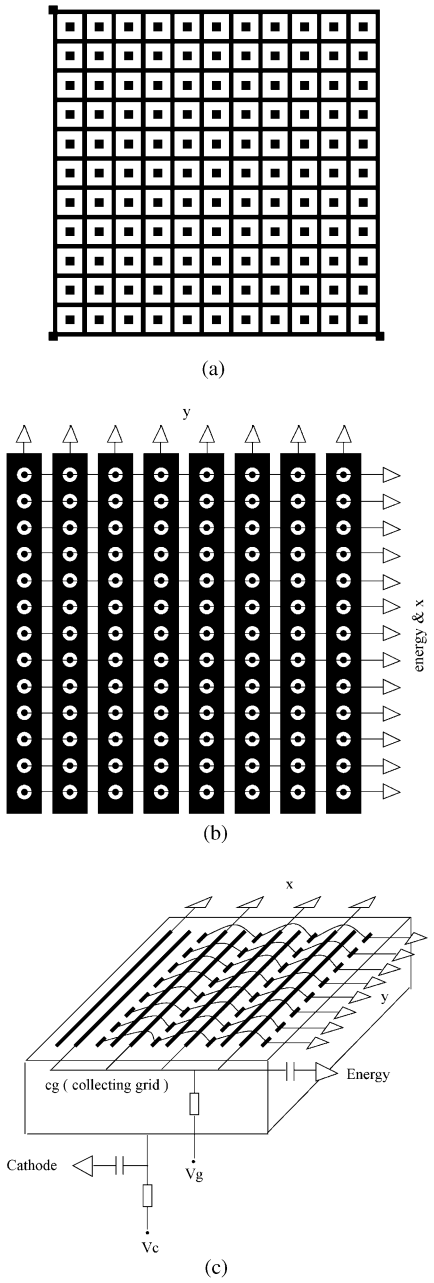

Fig. 5. Illustration of 3-D position sensitive semiconductor devices. (a) Pixellated anode array used by He et al. [35]. (b) Schematic of anode array suggested by Hamel et al. [39]. (c) Illustration of a device suggested by Luke et al. [41].

Section 2.5, three-dimensional coordinates of each γ-ray interaction can be obtained together with the energy deposition. Therefore, the variation of pulse amplitude due to the variation of charge trapping, material non-uniformity and gain variation of the readout electronic circuitry can be corrected to the limit of position resolution in 3-D. The challenge is to read out a large number of independent channels. Recent development in application specific integrated circuitry (ASIC) makes the data acquisition possible. This 3-D position sensing method offers some unique advantages: (1) 3-D position sensing could be critical to some γ-ray imaging applications [36]. (2) It can correct for material non-uniformity on wide band-gap semiconductors, to the extent of position resolution [37,38]. (3) It can result in the minimum electronic noise because the total leakage current is shared among a large number of anode pixels and the capacitance of each pixel electrode is minimized. (4) Since the variation of pulse amplitude can be corrected in 3-D, it is not necessary to compensate this variation using the shape of the weighting potential. Therefore, the design of the anode array, which is usually optimized for imaging applications and determines the weighting potentials of each anode pixel, can be independent of the operating voltage which determines the trapping of charge carriers.

Other 3-D position sensing techniques have been proposed. Hamel et al. [39] suggested a configuration that has an array of small anode pixels located along the center lines of parallel non-collecting anode strips as shown in Fig. 5(b). Anode pixels are interconnected along the orthogonal direction to the non-collecting anode strips and are biased at a higher potential. The energy and x coordinate are obtained from the pulse amplitude and the location of the rows of the collecting anode pixels, and y position is from the induced signal on the columns of the non-collecting anode strips. Since each row of collecting anode pixels are connected, the weighting potential of one row of anode pixels is very similar to that of an anode strip in the strip detector configuration discussed in Section 2.6, which is concentrated in the neighborhood of pixels along the row. The difference is that the increase of

the weighting potential in the region from $z = 0$ to $(1 - P)$ (P is roughly the dimension of one anode pixel here) is in general lower because the presence of the non-collecting anode strips between anode pixels forces the weighting potential to become zero between collecting anode pixels. The pulse amplitude on each row of collecting anode pixels is roughly proportional to the number of electrons collected. The variation of pulse amplitude due to charge trapping can be compensated by the shape of the weighting potential, note that the optimum compensation only occurs at a particular voltage between the cathode and the anode, or can be corrected by using depth sensing. The author proposed to obtain the depth of γ-ray interaction from the negative pulse amplitude derived from the non-collecting anode strips. The challenges of implementing this technique are: (1) To obtain good signal-to-noise ratio (SNR) from the non-collecting anode strips. When electrons enter the neighborhood of a non-collecting anode strip, they induce a transient signal which intrinsically has much poorer SNR than that on the collecting anode pixels. The poorer SNR causes higher energy thresholds on the non-collecting anode strips than on the collecting anode pixels. This means the loss of Y coordinates for low energy events. (2) Poorer SNR from non-collecting anode strips could limit depth resolution if signals from non-collecting strips were used, especially on thick (detector thickness $\gg$ strip pitch) detectors. If the signal from only one non-collecting anode were to be used, the weighting potential of a single anode strip changes slowly (not sensitively) in the region $0 \leqslant z \leqslant 1 - P$, so that the signal changes only mildly as a function of depth. If signals from multiple non-collecting anodes were to be used, the signal amplitude changes more sensitively as a function of depth, but the noise would also increase from the required multi-channel read out. Position sensing on this type of detector has been demonstrated using α particles [40]. Measurements using low energy γ-rays, which will induce a much lower signal amplitude, have yet to be studied.

Another method was proposed by Luke et al. [41]. The energy is read out from a single collecting anode as discussed in Section 2.4 [17]. The difference from the original single-electrode readout is that the loss of pulse amplitude due to electron trapping does not have to be compensated exactly, since it can be corrected from position sensing. The non-collecting anode is segmented to form two orthogonal arrays of electrodes shown in Fig. 5(c). The induced signals by electrons when they pass the neighborhood of elements of non-collecting anodes give the x and y coordinates. The depth of the γ-ray interaction is obtained from the ratio of signals of the cathode and the collecting anode as discussed in Section 2.5. Similar to Hamel's method, the challenge of implementing this technique depends mainly on obtaining good signal-to-noise ratio on the non-collecting anode signals, which is important to identify positions (x & y). This is due to the intrinsically poorer signal-to-noise ratio of transient signals compared to that of the collecting anode signal. This challenge is more significant for multiple energy depositions, such as a Compton scattering event. In these cases, multiple interaction positions need to be identified and individual energy depositions at each position need to be separated from the total energy signal from the collecting anode. The advantage over pixel anode array is a smaller number of readout channels ($\sim 2N$ versus N^2). However, all the bulk leakage current is collected on the collecting anode, therefore, the intrinsic noise from that source is higher than that using an anode array.

2.9. Summary

The Shockley–Ramo theorem is reviewed based on the conservation of energy. A variety of representative techniques employed with semiconductor γ-ray detectors have been summarized and discussed based on the Shockley–Ramo theorem. In analyzing many different schemes of readout techniques, an understanding and correct application of the Shockley–Ramo theorem are essential. A common feature of all types of single polarity charge sensing techniques is the rapid increase of the weighting potential in the vicinity of the collecting electrode. Since the weighting potential only changes from 0 to 1, it is thus very low in the region away from the collecting electrode. This

means that the movement of charge carriers away from the collecting electrode contributes very little to the induced signal. The most important progress in recent years on room-temperature semiconductor γ-ray spectrometers is to make use of the differences between the weighting potentials of different electrodes and the actual operating potential.

Acknowledgements

The author is very grateful for the suggestions and comments of Glenn F. Knoll and David K. Wehe.

References

[1] W. Shockley, Currents to conductors induced by a moving point charge, J. Appl. Phys. 9 (1938) 635.
[2] S. Ramo, Currents induced by electron motion, Proceedings of the I.R.E., September 1939, p. 584.
[3] C.K. Jen, On the induced current and energy balance in electronics, Proceedings of the I.R.E., June 1941, p. 345.
[4] G. Cavalleri et al., Extension of Ramo's theorem as applied to induced charge in semiconductor detectors, Nucl. Instr. and Meth. 92 (1971) 137.
[5] J.D. Jackson, Classical Electrodynamics, 2nd Edition, Wiley, New York, ISBN 0-471-43132-X.
[6] A. Maruhashi, Characteristics of a miniature dosimeter developed for measurement of electrons, Nucl. Instr. and Meth. A 141 (1977) 87.
[7] G.F. Knoll, Radiation Detection and Measurement, 3rd Edition, Wiley, New York, 2000. ISBN 0-471-07338-5.
[8] L.T. Jones, P.B. Woollam, Resolution improvement in CdTe γ detectors using pulse-shape discrimination, Nucl. Instr. and Meth. 124 (1975) 591.
[9] M. Richter, P. Siffert, High resolution γ-ray spectroscopy with CdTe detector systems, Nucl. Instr. and Meth. A 322 (1992) 529.
[10] H. Takahashi et al., Signal processing for CdTe detectors using a fast signal digitizing technique, Nucl. Instr. and Meth. A 380 (1996) 381.
[11] O. Frisch, British Atomic Energy Report BR-49, 1944.
[12] P.N. Luke, Single-polarity charge sensing in ionization detectors using coplanar electrodes, Appl. Phys. Lett. 65 (1994) 2884.
[13] P.N. Luke, Unipolar charge sensing with coplanar electrodes—application to semiconductor detectors, IEEE Trans. Nucl. Sci. NS-42 (4) (1995) 207.
[14] Z. He, Potential distribution within semiconductor detectors using coplanar grid electrodes, Nucl. Instr. and Meth. A 365 (1995) 572.
[15] P.N. Luke, Electrode configuration and energy resolution in gamma-ray detectors, Nucl. Instr. and Meth. A 380 (1996) 232.
[16] K. Zanio, Use of various device geometries to improve the performance of CdTe detectors, Rev. Phys. Appl. 12 (1977) 343.
[17] M. Amman et al., Coplanar-grid detector with single-electrode readout, Proceedings of SPIE, Vol. 3115, 1997, p. 205.
[18] B.E. Patt et al., New gamma-ray detector structures for electron only charge carrier collection utilizing high-Z compound semiconductor, Nucl. Instr. and Meth. A 380 (1996) 276.
[19] J.F. Butler, Novel electrode design for single-carrier charge collection in semiconductor nuclear radiation detectors, Nucl. Instr. and Meth. A 396 (1997) 427.
[20] D.S. McGregor et al., CdZnTe semiconductor parallel strip Frisch grid radiation detectors, IEEE Trans. Nucl. Sci. NS-45 (3) (1998) 443.
[21] E.Y. Lee et al., Device simulation of a unipolar gamma-ray detector, Proceedings of MRS, Vol. 487, 1998, p. 537.
[22] D.S. McGregor et al., Geometrically weighted semiconductor Frisch grid radiation spectrometers, Nucl. Instr. and Meth. A 422 (1999) 164.
[23] Z. He et al., 1-D position sensitive single carrier semiconductor detectors, Nucl. Instr. and Meth. A 380 (1996) 228.
[24] Z. He et al., Position-sensitive single carrier CdZnTe detectors, Nucl. Instr. and Meth. A 388 (1997) 180.
[25] Z. He et al., Coplanar grid patterns and their effects on energy resolution of CdZnTe detectors, Nucl. Instr. and Meth. A 411 (1998) 107.
[26] M. Amman, P. Luke, Optimization criteria for coplanar-grid detectors, IEEE Trans. Nucl. Sci. NS-46 (3) (1999) 205.
[27] J.M. Ryan et al., Large area sub-millimeter resolution CdZnTe strip detectors for astronomy, Proc. SPIE 2518, p. 292, 1995.
[28] C.M. Stahle et al., CdZnTe strip detectors for arc second imaging and spectroscopy, Proceedings of SPIE, Vol. 2859, 1996, p. 74.
[29] A. Parsons et al., Performance of prototype segmented CdZnTe arrays, Proceedings of MRS, Vol. 487, 1998, p. 147.
[30] F.P. Doty et al., Pixellated CdZnTe detector arrays, Nucl. Instr. and Meth. A 353 (1994) 356.
[31] H.B. Barber et al., Progress in developing focal-plane-multiplexer readout for large CdZnTe arrays for nuclear medicine applications, Nucl. Instr. and Meth. A 380 (1996) 262.
[32] H.H. Barrett et al., Charge transport in arrays of semiconductor gamma-ray detectors, Phys. Rev. Lett. 75 (1995) 156.
[33] A. Shor et al., Spectroscopy with CdZnTe γ- and X-ray detectors by modifying the electron trapping to compensate for incomplete charge collection caused by large hole trapping, Nucl. Instr. and Meth. A 426 (1999) 491.

[34] W.R. Cook et al., First test results from a high resolution CdZnTe pixel detector with VLSI readout, Proceedings of SPIE, July 18–23, Denver, CO, 1999.
[35] Z. He et al., 3-D position-sensitive CdZnTe gamma-ray spectrometers, Nucl. Instr. and Meth. A 422 (1999) 173.
[36] Y.F. Du et al., Evaluation of a compton scattering camera using 3-D position sensitive CdZnTe detectors, Proceedings of SPIE, July 18–23, Denver, CO, USA, 1999.
[37] W. Li et al., Spatial variation of energy resolution in 3-D position sensitive CZT gamma-ray spectrometers, IEEE Trans. Nucl. Sci. NS-46 (3) (1999) 187.
[38] Z. He et al., Measurement of material uniformity using 3-D position sensitive CdZnTe gamma-ray spectrometers, Nucl. Instr. and Meth. A 441 (2000) 459.
[39] L.A. Hamel et al., An imaging CdZnTe detector with coplanar orthogonal anode strips, Proceedings of MRS, Vol. 487, 1998, p. 211.
[40] O. Tousignant et al., Energy and position resolution of a CdZnTe γ-ray detector with orthogonal coplanar anodes, Proceedings of SPIE, July 18–23, Denver, CO, USA, 1999.
[41] P.N. Luke et al., Coplanar grid CdZnTe detectors with three-dimensional position sensitivity, Nucl. Instr. and Meth. A 439 (2000) 611.